



HAL
open science

Break-in Bad: on the Conditioning of Fuel Cell Nanoalloy Catalysts

Raphaël Chattot, Camille Roiron, Kavita Kumar, Vincent Martin, Carlos Augusto Campos Roldan, Marta Mirolo, Isaac Martens, Luis Castanheira, Arnaud Viola, Rémi Bacabe, et al.

► **To cite this version:**

Raphaël Chattot, Camille Roiron, Kavita Kumar, Vincent Martin, Carlos Augusto Campos Roldan, et al.. Break-in Bad: on the Conditioning of Fuel Cell Nanoalloy Catalysts. *ACS Catalysis*, 2022, 12 (24), pp.15675–15685. 10.1021/acscatal.2c04495 . hal-03887640

HAL Id: hal-03887640

<https://hal.science/hal-03887640>

Submitted on 8 Nov 2023

HAL is a multi-disciplinary open access archive for the deposit and dissemination of scientific research documents, whether they are published or not. The documents may come from teaching and research institutions in France or abroad, or from public or private research centers.

L'archive ouverte pluridisciplinaire **HAL**, est destinée au dépôt et à la diffusion de documents scientifiques de niveau recherche, publiés ou non, émanant des établissements d'enseignement et de recherche français ou étrangers, des laboratoires publics ou privés.



Distributed under a Creative Commons Attribution 4.0 International License

Break-in Bad: on the Conditioning of Fuel Cell

Nanoalloy Catalysts

*Raphaël Chattot^{1, *}, Camille Roiron², Kavita Kumar², Vincent Martin², Carlos Augusto Campos Roldan¹, Marta Mirolo³, Isaac Martens³, Luis Castanheira⁴, Arnaud Viola², Rémi Bacabe¹, Sara Cavaliere^{1,5}, Pierre-Yves Blanchard¹, Laetitia Dubau², Frédéric Maillard² and Jakub Drnec³*

¹ ICGM, Univ. Montpellier, CNRS, ENSCM, 34095 Montpellier Cedex 5, France

² Univ. Grenoble Alpes, Univ. Savoie Mont Blanc, CNRS, Grenoble INP*, LEPMI, 38000 Grenoble, France. *Institute of Engineering and Management Univ. Grenoble Alpes

³ ESRF, The European Synchrotron, 71 Avenue des Martyrs, CS40220, 38043 Grenoble Cedex 9, France

⁴ Symbio, 14 Rue Jean-Pierre Timbaud, Espace des Vouillands 2, 38600 Fontaine, France

⁵ Institut Universitaire de France (IUF), 75231 Paris Cedex 5, France

*e-mail: (RC) raphael.chattot@umontpellier.fr;

KEYWORDS: Nanocatalysts, Fuel Cell, Conditioning, Operando X-ray Diffraction, Online ICP-MS

ABSTRACT

Fuel cell catalysts preliminary testing in model laboratory environment is an essential step in the technology readiness level progression of material candidates toward the commercial device. However, in the case of platinum alloy catalysts for the oxygen reduction reaction (ORR) in proton exchange membrane fuel cells (PEMFC), there is no consensus on the protocol employed for catalyst conditioning (activation, or break-in), leading to important discrepancies in the literature.

Here, the effects of electrochemical conditioning on PtNi nanocatalysts structure, chemical composition and performance for the ORR are investigated using *operando* high energy X-ray diffraction in both liquid electrolyte and X-ray transparent PEMFC, on-line inductively coupled plasma mass spectrometry (ICP-MS) and the rotating disk electrode (RDE) techniques. Our results show that for PtNi/C materials, the cost in ORR performance associated to complete surface stabilization at the potential of the ORR can be dramatic, but also mitigated by adjusting the initial chemistry and structure of the catalyst. Overall, this study reveals how incomplete catalyst conditioning in RDE leads to highly erroneous conclusions regarding its performance and stability to be possibly found in realistic PEMFC device, and proposes simple strategies to close this gap.

INTRODUCTION

Nanocatalysts play a critical role in the performance, cost and lifetime of numerous fuel cell technologies. This is particularly true for the proton-exchange membrane fuel cell (PEMFC), where the combined highly corrosive environment and mechanism complexity of the cathodic oxygen reduction reaction (ORR) mostly imposes the use of noble, scarce and expensive platinum (Pt) group metal-based catalysts. Consequently, significant research effort at the fundamental level is dedicated to the design of cost-effective materials able to boost the widespread development of PEMFC in numerous industrial sectors. To date, numerous nanostructures of Pt alloyed with one or several early or late transition metal element(s) have shown tremendous improvements in catalytic properties for the ORR, even far above the commercial performance targets, when tested in thin-film-(rotating) disk electrodes configuration at the laboratory scale ¹.

A thin-film-(rotating) disk electrode (thin-film on RDE) is the simplified, idealized version of half a fuel cell. It allows rapid screening of new catalysts activity and stability from only few quantities of material at the early stage of development, prior to further larger-scale production and subsequent more extensive *in situ* evaluation in complete fuel cell. Especially, such characterization in liquid electrolyte prevents from the rather complex membrane electrode assembly (MEA) manufacturing, which requires specific laboratory equipment and expertise ²⁻⁵. This technique provides a truly intrinsic property of the catalyst, that is the kinetic current density for the ORR at a given electrode potential. This property is usually corrected from oxygen mass transport limitation and ohmic drop losses ‘artifacts’, that are more dependent on the electrochemical cell design and configuration than the catalyst itself. This should in principle favor general agreement between research groups when assessing the catalyst ORR performance. In that frame, numerous seminal works have evidenced the extreme sensitivity of the kinetic current density for the ORR to the experimental conditions ^{4,6-9}, and established the ‘best practices’ regarding the thin-film electrode preparation, glassware cleanliness, purity of the chemicals or catalytic ink composition and formulation toward more reliable and reproducible results.

However, there is still no clear consensus in the RDE literature regarding the testing protocol for the very first step of nanocatalyst electrochemical characterization that is electrochemical conditioning (also referred as activation or break-in), whereas it is gaining considerable attention at the device level ¹⁰⁻¹². The tacitly accepted common approach with RDE consists in repetitive electrode potential cycling until the cyclic voltammograms (CVs) become stable. Shinozaki *et al.* ⁶ conducted one of the rare systematic studies on the impact of conditioning protocol, notably regarding the effects of potential scan rate and upper potential limit on the specific activity of polycrystalline bulk electrode (poly-Pt) and Pt/C catalyst. These authors suggest that since scan rates in the range 100-500 mVs⁻¹ produce similar outcomes over 50 cycles, 500 mVs⁻¹ has the advantage of requiring less time. Complementarily, it was revealed that upper potential limit of only 1.0 V vs. the Reversible Hydrogen Electrode (RHE) resulted in incomplete conditioning of both poly-Pt and Pt/C, while reaching 1.2 or even 1.4 V vs. RHE was found necessary for complete contaminant removal from the surface and maximization of the electrochemically active surface area (ECSA). Nonetheless, by taking into consideration the issue of carbon corrosion in Pt/C catalyst at such high potential, 1.2 V vs. RHE as upper limit was found to represent a satisfactory compromise between catalyst surface cleanliness and structural integrity.

Now, the question of how these findings transpose to more complex PtM/C nanostructures (where M is an early or late transition metal) currently investigated by the RDE literature is still largely open. Clearly, reaching satisfactory surface cleanliness while preventing the dissolution of non-noble elements (Ni, Co, Cu, etc.) is the main challenge in this case. Especially, in the context where the conditioning step aims at reaching a defined and stable initial surface state, should the dissolution of highly unstable surface and subsurface M species (even at the detriment of the catalyst activity) be part of the conditioning step in RDE experiments? These considerations are of primary importance when considering the distinction with conditioning procedures used in realistic PEMFC devices, that range from hours to days to perform ¹³. In fact, reaching complete conditioning in PEMFC means reaching stable (and if possible maximum) cell performance, but contrary to the RDE configuration, this performance depends not only on the catalyst

surface state but also largely on other parameters of the membrane electrode assembly (MEA), such as membrane and ionomer hydration that impact proton conductivity. In other words, to pass PEMFC conditioning, reaching *stable* catalyst surface state and intrinsic activity is necessary, while reaching *maximum* intrinsic activity is not sufficient. Especially, numerous works reported on the collateral damages from PEMFC conditioning to the catalyst layers^{10,14,15}. Among others (temperature, gas atmosphere *etc.*), possible distinction between the RDE and PEMFC conceptions of this very first step of activation would likely contribute to the extreme discrepancies observed between PtM/C catalysts performance screened by the RDE and their practical performance in PEMFC^{16,17}. Note that in view of addressing the main shortcomings of the RDE setup (unrealistic liquid electrolyte, low current density due to low reactant concentration *etc.*), the literature is now dedicating raising attention to the Gas Diffusion electrode (GDE) setup¹⁸⁻²³. Because the current ‘best practices’ in this case, notably regarding electrocatalyst break-in, are based on RDE-like electrode cycling protocol¹⁸, the above-mentioned questioning extends to the GDE setup.

In this contribution, the effects of electrochemical conditioning on PtNi nanocatalyst structure, chemical composition and performance for the ORR are investigated using *operando* high energy X-ray diffraction in both liquid electrolyte and solid electrolyte X-ray transparent PEMFC, on-line inductively coupled plasma mass spectrometry (ICP-MS) and rotating disk electrode (RDE) techniques, respectively. The sequential effects of two conditioning protocols are investigated on a material’s library composed of a commercial Pt/C catalyst (20 wt. %, Tanaka Kikinzoku Kogyo, TKK), and two in-house catalysts that are faceted PtNi-rich/C (high Ni content) nanoparticles and PtNi-poor/C (low Ni content) nanosponges. Our results show how the conclusions previously obtained on poly-Pt and Pt/C surfaces extend to PtNi/C materials, and identify the conditioning step as a major source of discrepancy between catalyst performance and stability screened by the RDE and possibly observed in realistic PEMFC device. They also provide simple guidelines to be implemented in RDE testing to solve this issue.

TEXT

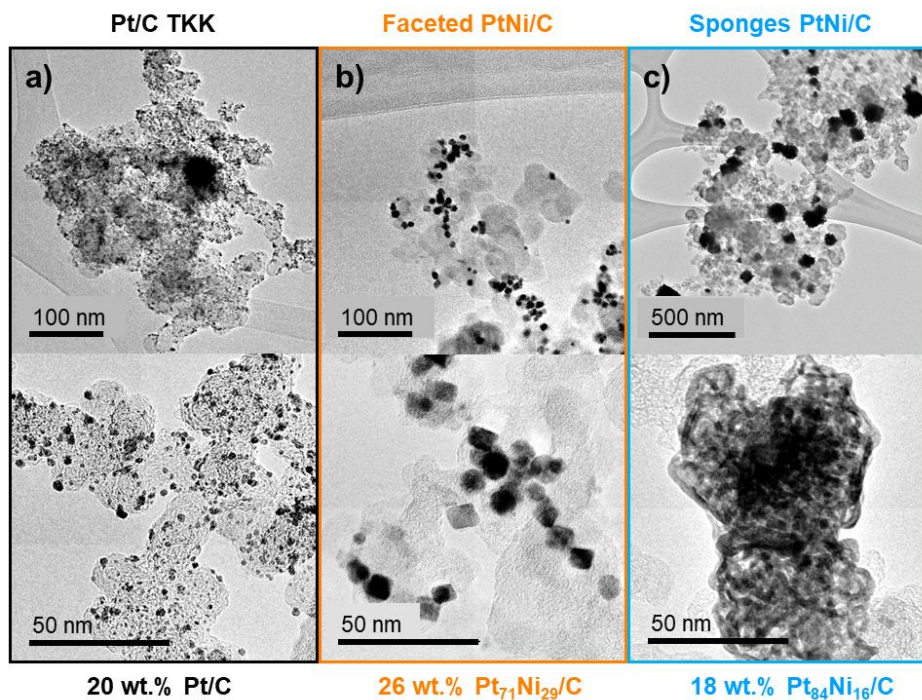


Figure 1: TEM images and chemical composition of (a) Pt/C TKK reference catalyst, (b) Faceted PtNi/C catalyst and (c) Sponges PtNi/C catalyst. The global Pt weight fraction was estimated from ICP-MS and the chemical composition of the nanoparticles estimated from the lattice constant measured by Rietveld refinement of initial WAXS patterns and Vegard's law.

Figure 1 shows transmission electron microscopy (TEM) images of the three catalysts investigated in this study with their corresponding Pt weight fraction (wt. %) and Pt:Ni chemical composition. Because the global chemical composition of the samples does not necessarily correspond to the composition of the nanoparticles (possible traces of pure Ni non alloyed with Pt, see **Figure S1** of the **Supporting Information**) the Pt wt. % was determined by ICP-MS, but the Pt:Ni composition of the nanoparticles was determined from Rietveld refinement of the *ex situ* wide angle X-ray scattering (WAXS) patterns and the Vegard's law (see **Table S1** of the **Supporting Information**). Compared to the reference Pt/C TKK catalyst displayed in **Figure 1.a** composed of *ca.* 1-2 nm pure Pt nanoparticles, the first in-house PtNi/C material consists in large (*ca.* 8 nm) nanoparticles featuring 29 Ni at.% alloyed with Pt. As visible in **Figure 1.b**, this sample features a large fraction of faceted nanoparticles mixing cubic and octahedral shapes, and will

be referred in the following as ‘Faceted PtNi/C’. An important note for the following is that this sample has been thoroughly washed with toluene, ethanol and deionized water but not acid washed after the synthesis (see **Experimental Methods**). The third catalyst investigated is an original PtNi/C material we introduced and described in previous contributions²⁴⁻²⁶, referred here as ‘Sponges PtNi/C’. Compared with the Faceted PtNi/C sample, this catalyst is composed of large (*ca.* 50-60 nm) nanoporous multi-grained superstructures, themselves composed of *ca.* 5 nm PtNi nanocrystallites (**Figure 1.c**). Also, the Sponges PtNi/C sample features a lower content of 16 Ni at.%, notably because of the acidic treatment performed at the last step of the synthesis (22 h in 1 M H₂SO₄, see **Experimental Methods**). Overall, the PtNi/C catalysts investigated represent two different strategies toward enhanced ORR kinetics largely discussed in previous contributions^{25,27}. Briefly, Faceted PtNi/C material is based on either the presence of alloyed Ni in surface or near surface regions of the catalyst to tune its surface electronic structure²⁸, while the Sponges PtNi/C material relies on the use of Ni as a sacrificial element (dealloying) for the implementation of nanoporosity and surface distortion with desirable effects on ORR kinetics^{24,25,29}. Importantly, the catalytic site coordination is tuned at the global scale by faceting in the case of Faceted PtNi/C³⁰, while it is tuned locally for the Sponges PtNi/C by the presence of structural defects³¹.

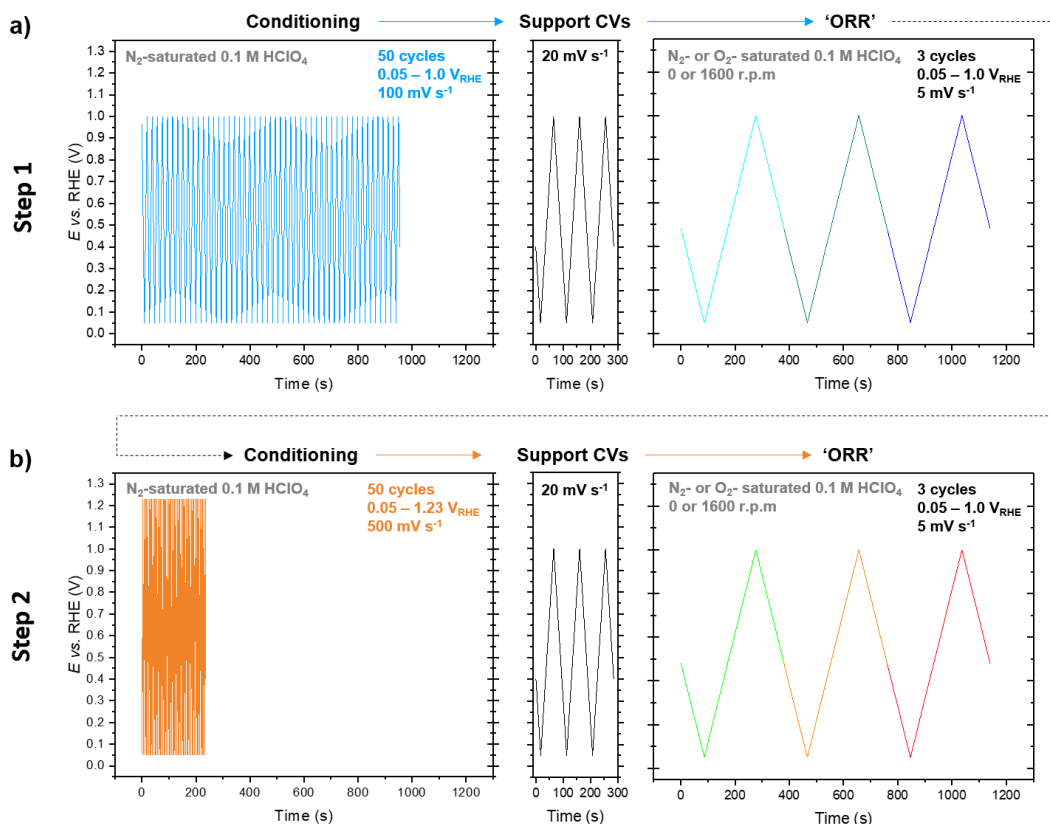


Figure 2: Experimental protocol for operando WAXS, online ICP-MS and RDE investigations. For the operando WAXS and online ICP-MS, the simulated 'ORR' steps were investigated under O_2 -free 0.1 M $HClO_4$ on stationary electrode, while the RDE was performed in O_2 -saturated 0.1 M $HClO_4$ with an electrode rotation speed of 1600 r.p.m. Step 1 (a) and Step 2 (b) were performed sequentially on the same electrode for operando WAXS and online ICP-MS, while O_2 was introduced only after Step 1 or after Step 1+2 on separated electrodes for RDE measurements. For all experiments, the electrodes loadings were $20 \mu g_{Pt} cm^{-2}$.

Figure 2 depicts the experimental protocol followed in this study for operando WAXS, online ICP-MS and RDE investigations. The samples were sequentially subjected to two main steps, each one consisting in a conditioning protocol, CVs in support electrolyte and (simulated) ORR measurements. During Step 1 (**Figure 2.a**), the conditioning consisted in 50 potential cycles at 100 mV s^{-1} in O_2 -free 0.1 M $HClO_4$ between 0.05 V vs. RHE and 1.0 V vs. RHE. Then, three support CVs in O_2 -free 0.1 M $HClO_4$ were recorded between 0.05 V vs. RHE and 1.0 V vs. RHE at 20 mV s^{-1} . Step 1 ends with three 'ORR' measurement cycles in quasi-stationary state, *i.e.* between 0.05 V vs. RHE and 1.0 V vs. RHE at 5 mV s^{-1} . Importantly, because operando WAXS and online ICP-MS measurements were not technically possible on rotating electrode

with our setups, the ‘ORR’ were simulated in N₂-saturated electrolyte and stationary thin-film electrode, while O₂ and electrode rotation (1600 r.p.m.) were introduced in the RDE tests. This compromise in WAXS and online ICP-MS experiments still allows quantifying the catalyst structural stability at electrode potential relevant for the ORR after a given conditioning step, but the possible influence of oxygen present in solution is not captured (but was found insignificant for Pt(111) surface within such electrode potential range³²). Step 2 (**Figure 2.b**) is similar to Step 1, except the conditioning part consisted in 50 potential cycles at 500 mV s⁻¹ in O₂-free 0.1 M HClO₄ between 0.05 V vs. RHE and 1.23 V vs. RHE (directly inspired from the recommendations of Shinozaki *et al.* for Pt surfaces⁶). Step 1 and Step 2 were performed sequentially on the same electrode for *operando* WAXS and online ICP-MS, while O₂ was introduced for ORR measurements only after Step 1 or after Step 1+2 on separated electrodes during RDE tests. CO-stripping measurements were performed at last, after ORR measurements. Overall, this protocol ensures strictly similar electrode history between ORR activity measurements and *operando* characterization. The *operando* WAXS patterns were measured during simulated ORR polarization cycles on thin-films electrodes loaded with 20 μg_{Pt} cm⁻² (as for online ICP-MS and RDE experiments) of the different catalysts with a temporal resolution of *ca.* 350 ms. The measurements were performed in grazing incidence configuration in a three-electrode electrochemical flow cell (see **Figure S2**). The quantification of Pt and Ni dissolution in acidic media at room temperature during Step 1 or Step 1+2 was investigated using a three-electrode electrochemical flow cell coupled to an ICP-MS presented in a previous contribution³³. More details are provided in the **Experimental Methods** section of the **Supporting Information**

The impact of the different conditioning steps on the catalysts surface can be first attested by the conventional approach, *i.e.* by analyzing the shape and the stability of the support CVs in **Figure 3.a-c**. Clearly, and for both Pt and PtNi materials, the conditioning procedure composed of 50 potential cycles at 100 mV s⁻¹ between 0.05 V vs. RHE and 1.0 V vs. RHE (Step 1) allows reaching highly reproducible CVs in the same potential range at lower sweep rate, as attested by the superimposition of the three consecutive cycles (cyan, dark cyan and blue traces in **Figure 3.a-c**). Interestingly, however, performing additional 50

potential cycles at 500 mV s^{-1} between 0.05 V vs. RHE and 1.23 V vs. RHE (Step 2) also leads to stable and superimposed CVs (green, orange and red traces in **Figure 3.a-c**) but slightly different than the ones obtained after Step 1. In the case of the reference Pt/C TKK in **Figure 3.a**, one can observe a significant increase of the electrical charges associated with adsorption and desorption of both under-potentially deposited hydrogen (referred as H_{UPD} in the following) and surface oxides. This is in agreement with the results from Shinozaki *et al.* on Pt surfaces⁶, confirming that the upper potential limit of 1.23 V vs. RHE leads to a better removal of surface contaminants compared to 1.0 V vs. RHE , possibly accompanied with surface reconstruction, as pointed out by studies on single crystals^{34,35}. The question of the nature of such electroinactive species adsorbed on the catalyst surface (referred to as ‘crap on the electrode’ by A. Bard³⁶) is still largely open, but both mineral or organic residues from nanocatalyst synthesis media (oleylamine, oleic acid, ethylene glycol *etc.*) are probable candidates here, and inherent to practical nanocatalysts. Whereas the changes in the H_{UPD} amplitude preserve its shape, this is not the case at higher potentials. In fact, one can also observe a *ca.* 30 mV decrease on the onset of surface oxide formation, associated with a pronounced tailing in their subsequent reduction to a potential as low as 0.4 V vs. RHE . This suggests that the catalytic sites ultimately ‘cleaned’ by the further conditioning of Step 2 are in average more oxophilic than the free sites after Step 1.

In the case of PtNi materials, the observed trends depend on the catalyst structure. As for Pt/C TKK, the surface of Faceted PtNi/C (**Figure 3.b**) appears also cleaner and more oxophilic after Step 1+2 compared to after Step 1. Clearly, the electrical currents associated to formation and reduction of surface oxides that were mostly disabled in this electrode potential range after Step 1, are visible after Step 1+2. Interestingly, these changes are highly asymmetrical (similar oxidative current but increased reduction current), suggesting a possible transition from a faradaic oxidation of residual contamination after Step 1 toward a ‘reversible’ Pt oxidation after Step 1+2. Finally, the acid-leached Sponges PtNi-poor/C show only minor changes in the CVs after Step 1 and after Step 1+2 (**Figure 3.c**). Still, the plateau in oxidative current at high potential observed after Step 1+2 suggests better surface cleanliness compared to after Step 1. Also,

the shape of the H_{UPD} slightly evolves, with the development of a peak at potential higher than 0.30 V vs. RHE. This feature has been previously associated to an electrochemical signature of surface lattice distortion²⁶, which are implemented by design for this electrocatalyst. According to the CVs experiments, the necessity in surpassing 1.0 V vs. RHE during conditioning for complete contaminants removal on Pt/C seems to also apply for PtNi/C materials. However, whether the changes observed in the CVs of PtNi materials are caused only by contamination removal and/or changes in Pt:Ni surface composition and reconstruction remains unknown at this stage. Importantly, the apparent stability (reproducibility) of the support CVs recorded at 20 mV s⁻¹ (for example here after Step 1) is no evidence for complete conditioning.

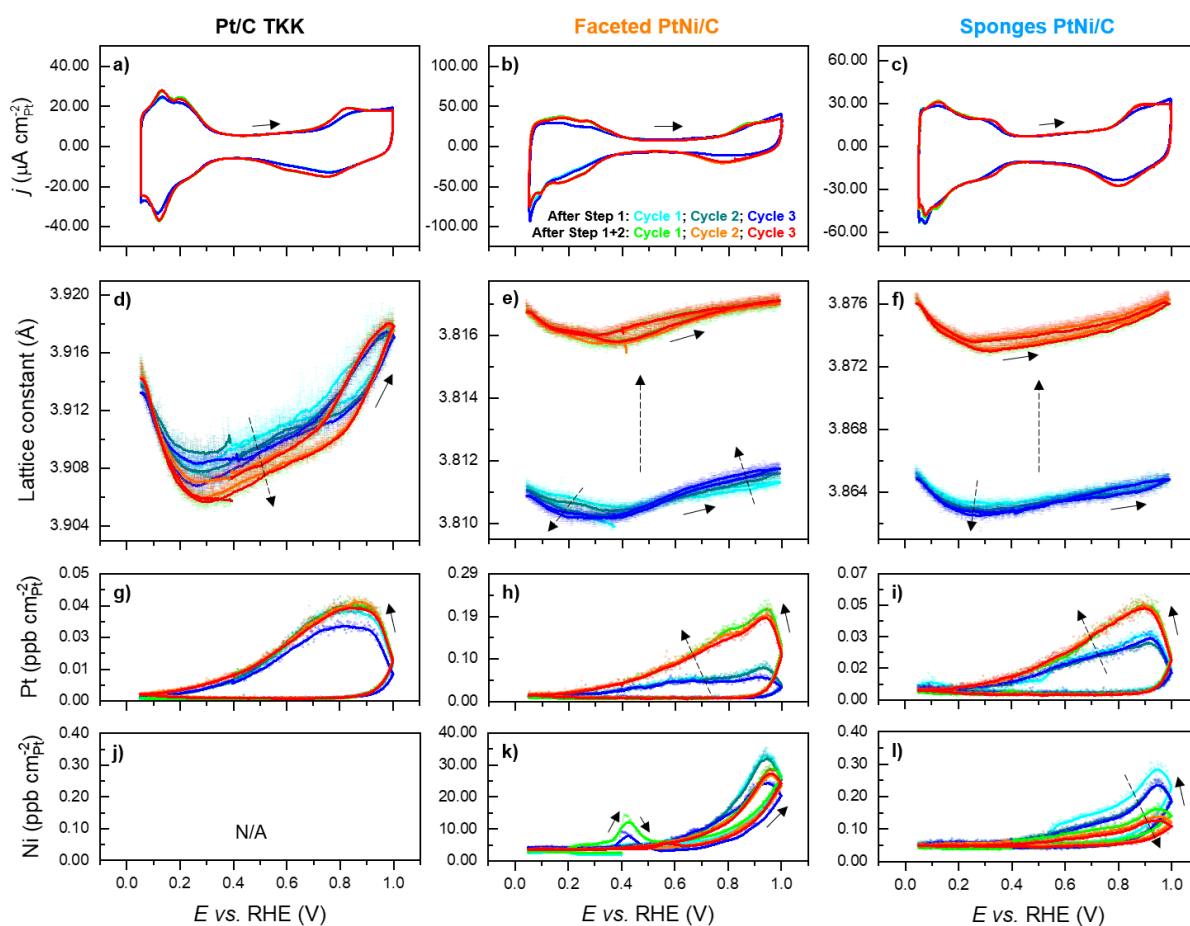


Figure 3: Three first consecutive cycles of a)-c) support CVs measured at 20 mV s⁻¹ with RDE; d)-f) lattice strain dynamics measured with operando WAXS; g)-i) Pt dissolution and j)-l) Ni dissolution measured with online ICP-MS after Step 1 (cyan, dark cyan and blue traces) and Step 1+2 (green, orange and red traces) for Pt/C TKK, Faceted

PtNi/C and Sponges PtNi/C catalysts. The electric current is normalized by the CO_{ads} -stripping charge measured at the end of Step 1+2. In d)-l), the solid lines are adjacent-averages (30 pts window) of the raw datapoints displayed with transparency for easier reading.

Operando WAXS and online ICP-MS allow to see beyond the previously discussed support CVs, and to directly address the questions of material adsorption trends, structural and chemical integrity in the ORR potential range during simulated quasi steady-state conditions. Rietveld refinement of the WAXS patterns was used to reveal the electrochemical strain dynamics (variations of the lattice constant) during three consecutive cycles of electrode polarization at 5 mV s^{-1} after the different conditioning steps (**Figure 3.d-f**). As discussed in details in dedicated previous contributions^{37,38}, the enhanced surface-to-volume ratio of nanoparticles allows adsorption processes to be monitored by ‘bulk’ X-ray diffraction technique. Briefly, the lattice constant of Pt nanoparticles was found minimum (maximum compressive strain) at the potential of zero total charge (pztc), where the surface is (rather) free of adsorbates. Excursion of the electrode potential below (or above) the pztc resulted in a homogeneous increase of the lattice constant over the nanoparticle volume, associated with cations (or anions) adsorption processes. Note that the double-layer charging was found to also contribute as a background in the observed lattice expansion. In the present case of PtNi alloys, the absolute values of the lattice constant also inform on the fraction of Ni being alloyed with Pt according to the Vegards’ law. In this context, **Figure 3.d-f** unambiguously reveals the dramatic effects of the two conditioning steps regarding catalysts surface structural stabilization and/or integrity in the potential range of the ORR. In fact, the lattice strain dynamics is found not reproducible for any of the catalysts after Step 1, whereas Step 1+2 leads to highly reproducible trends for all the catalysts. This further confirms that even stable CVs between 0.05 and 1.0 V vs. RHE at 20 mV s^{-1} (far from the steady state) obtained after Step 1 do not necessarily ensure structural stability at 5 mV s^{-1} in the same potential range. Looking first at the reference Pt/C TKK in **Figure 3.d**, the lattice constant tends to decrease from one cycle to the next (cyan, dark cyan and blue traces), mostly in the so-called double-layer potential region (from 0.30 to 0.60 V vs. RHE). In agreement with the support CVs, this suggests the progressive removal of the residual contaminants or surface oxides still adsorbed on the surface. Structural data acquired after Step

1+2 (green, orange and red traces), on the contrary, show excellent reproducibility over three cycles. Compared to after Step 1, the lattice strain dynamics after Step 1+2 shows a sharp hysteresis above 0.20 V *vs.* RHE, confirming the above-mentioned hypothesis of highly oxophilic sites (the ones more prone to contamination) to be finally electrochemically active at this stage. These sites are found to be reduced only at potential as low as 0.20 V *vs.* RHE, ultimately supporting the idea that some features in the ‘ H_{UPD} ’ are in fact associated to oxides reduction and/or oxidation³⁹⁻⁴³.

Now looking at the potential-resolved online ICP-MS data of Pt/C TKK measured in similar conditions in **Figure 3.g**, and in agreement with pioneer work using online ICP-MS⁴⁴, Pt mostly dissolves during the cathodic sweep of the cycling voltammogram (descending potential). This cathodic dissolution is attributed to the reduction of sub-surface oxygen species formed at high electrode potential according to the place-exchange mechanism⁴⁵. However, the two sequential conditioning steps do not seem to impact the Pt dissolution trends in the potential region of the ORR in the case of Pt/C TKK (except the unexplained, peculiar case of the third cycle after Step 1).

Regarding the PtNi/C materials, the structural stabilization is accompanied with important transformations. In the case of Faceted PtNi/C in **Figure 3.e**, the lattice strain dynamics after Step 1 shows interesting features. First, the reversibility in lattice increase at high potential seems to be dominated by charges accumulation in the double-layer without pronounced hysteresis, suggesting the absence of significant oxidation of the surface at this stage. Second, as the ‘ORR’ cycles proceed after Step 1, the lattice parameter tends to contract at each subsequent cycle below 0.40 V *vs.* RHE and to expand above 0.60 V *vs.* RHE. While the contraction of the lattice at low potential is somehow similar to the observation on pure Pt/C TKK during contaminant removal, the expansion of the lattice at higher potential is unique to the Ni-rich Faceted PtNi/C material, and could likely be attributed to Ni leaching from the surface. In fact, stable structural data obtained after Step 1+2 confirms Ni leaching occurs in the process of catalyst structural stabilization, as the lattice constant shift from 3.8095 Å (fresh) to *ca.* 3.8102 Å (after Step 1) to 3.8160 Å (after Step 1+2). If these fine shifts in lattice parameter are well-captured by our experimental setup, they

only correspond to overall minor changes in Pt:Ni composition. According to the Vegards' law, the Faceted PtNi/C alloy sample experiences a loss of 0.7 % and 5.6 % of its initial Ni content after Step 1 and Step 1+2, respectively. Ni leaching is also detected by ICP-MS and integrations of the dissolution signals measured during the two Steps of the experimental protocol **Figure S3-S6**, and indicates that *ca.* 4 % and 7 % of the initial Ni content was lost after Step 1 and Step 1+2, respectively. However, the XRD method is concerning only Ni alloyed with Pt, while ICP-MS also detects the dissolution of the pure Ni phase present in this sample. The reproducible structural state dynamics of Faceted PtNi/C reached after Step 1+2 over the potential range of the ORR shows the presence of quasi-irreversible Pt oxidation (hysteresis) and a more pronounced lattice expansion in the H_{UPD} region, both suggesting a decrease of the alloying effects regarding weakened adsorption of hydrogen and oxide species. Online ICP-MS measurements of Pt dissolution in **Figure 3.h** confirm the dramatic changes in surface state, as the increased Pt oxidation revealed by WAXS data translates in a 2-fold increase of Pt dissolution rate. The ECSA-normalized Pt dissolution rate from the Faceted PtNi/C is 5-fold higher than from Pt/C TKK, suggesting high chemical instability (see ECSA values in **Table S1**). This instability can be at least partially explained by the Ni dissolution data in **Figure 3.j-k**, as the significant Ni dissolution from Faceted PtNi/C is likely to promote concomitant Pt dissolution⁴⁶. Finally, performing the second Step of conditioning only resulted in a mild decrease of the Ni dissolution rate. Note that the Ni dissolution peak around $E = 0.4$ V vs. RHE in **Figure 3.k** has been previously ascribed to the leaching of underpotentially-deposited Ni⁴⁷.

The trends observed on the Sponges PtNi/C are qualitatively close to the one observed for Faceted PtNi/C, except regarding Ni dissolution. Because the Sponges PtNi/C were previously dealloyed by acid washing post-synthesis, the lattice strain dynamics recorded after Step 1 is quite reproducible along three cycles (**Figure 3.f**). However, using a 1.23 V vs. RHE upper potential limit during the conditioning protocol still triggers further surface cleaning accompanied with Ni dissolution. The changes in lattice parameter are from 3.8610 Å (fresh) to *ca.* 3.8626 Å (after Step 1) to 3.8731 Å (after Step 1+2). This translates to a loss of 2.6 % and 20 % of their initial Ni content after Step 1 and Step 1+2, respectively. These values are

significantly higher than those observed for Ni-rich Faceted PtNi/C, suggesting the incapacity of small crystallites to retain even a low initial Ni content. The stable structural state reached by the Sponges PtNi/C shows strain dynamics qualitatively closer to Pt/C TKK than Faceted PtNi/C, except the amplitude of the oxidation irreversibility is much lower. Finally, Pt dissolution from the Sponges PtNi/C in **Figure 3.1** is almost identical to the Pt/C TKK. Most importantly, the Ni dissolution from the Ni-poor Sponges PtNi/C (**Figure 3.1**) in the potential range of the ORR is found nearly 200-fold below the one of Ni-rich Faceted PtNi/C.

Overall, the WAXS data further confirm and extend the necessity of ‘harsh’ conditioning protocol from Pt/C to PtNi/C materials, in order to reach at least temporary stable structural state in the ORR potential range. However, both WAXS and ICP-MS data indicate the conditioning of PtNi/C materials does not only relates to surface contaminants removal, but also largely alters surface chemical composition. Not surprisingly, Ni is leached during the catalyst’s stabilization process, and not only the vanishing of the alloying effects leads to more oxophilic surfaces and Pt dissolution rates, but also impacts the ORR performance, as shown below.

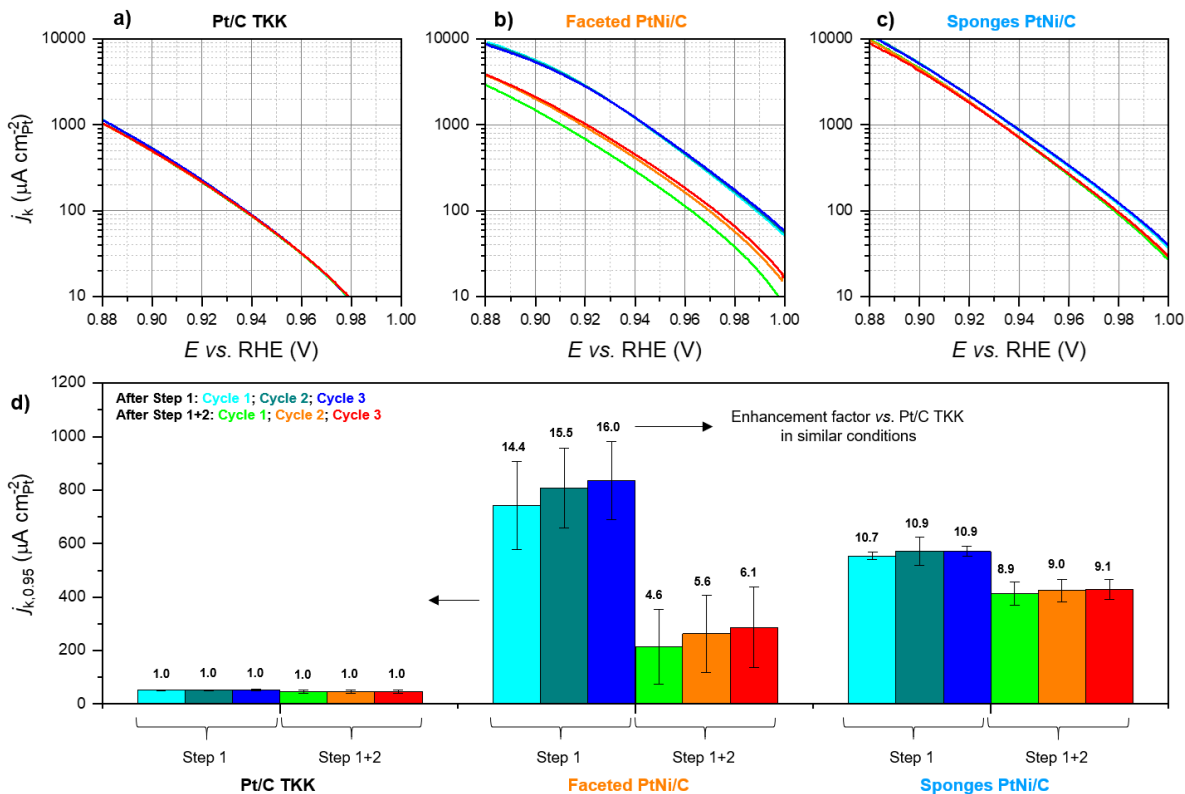


Figure 4: Impact of the conditioning steps and measurement cycle number on the estimated ORR kinetic current density with RDE. Tafel plot for the ORR for (a) Pt/C TKK; (b) Faceted PtNi/C and (c) Sponges PtNi/C. (d) ORR kinetic current density at 0.95 V vs. RHE. In (d), the numbers above the bars indicate the corresponding enhancement factors in ORR activity compared to Pt/C TKK in similar conditions (step and cycle). The kinetic current densities are corrected from the ohmic losses and O_2 mass transport limitation in solution. The error bars correspond to the standard deviations.

Figure 4 shows the impact of the different conditioning protocols (Step 1, or Step 1+2) also with the number of consecutive polarization cycle measurement (cycle 1, cycle 2 or cycle 3) on the values of ORR kinetic current density found for the different catalysts (see also **Table S2** and **Table S3**). Clearly, the trends displayed on the Tafel plots (**Figure 4.a-c**) are catalyst-dependent. In fact, reaching complete conditioning results in no significant change of the kinetic current density for the ORR for the reference Pt/C TKK, in a massive loss of performance for the Faceted PtNi/C material and to nearly no change for the Sponges PtNi/C. As quantitatively shown in **Figure 4.d**, from one step to the other, the ORR specific activity of Pt/C TKK, Faceted PtNi/C and Sponges PtNi/C decreases by 10 %, 71 % and 25%, respectively. In terms of

intrinsic activity enhancement factors values of PtNi materials compared to reference Pt/C TKK at similar state of conditioning (which is a convenient performance metric used between research laboratories), Faceted PtNi/C drops from 14.4 to 4.6 and Sponges PtNi/C from 10.7 to 8.9.

It appears thus clear that the question of whether the ORR activity from RDE is measured on a stable surface state or not is a complete game changer for PtM materials (M being a 3d transition metal), and must reach primary attention in the RDE literature. The danger in reporting ORR activity from highly unstable surface state is likely an overestimation of the catalyst performance to be found in the practical device after proper conditioning (due to transition metal leaching), but not only. In fact, performing consecutive ORR polarization curves at a given activation state allows attesting the relevance of a single point measurement. In the cases of pure Pt, the standard deviations associated with the six ORR activity measurements across the different states of conditioning is below 6 %, while they reach 15% and 40 % in case of acid-treated and untreated PtNi samples, respectively.

We finally propose a comparison of the two conditioning steps investigated here in RDE configuration and the structural degradation they produce with a fast conditioning protocol in single cell PEMFC device. Similar PtNi materials (Faceted PtNi/C and Sponges PtNi/C) were synthesized in larger batch quantities and integrated into 5 cm² membrane-electrode assemblies (MEAs) with Nafion 115 membrane, targeting 0.4 mg_{Pt} cm⁻² at the cathode. The MEAs were mounted inside a X-ray transparent PEM single cell ⁴⁸, allowing the acquisition of WAXS patterns of the cathode in *operando* conditions. The cell was operated at 353 K and 100 % relative humidity, and the anode and cathode sides were fed with 104 sccm H₂ and 250 sccm O₂, respectively, with 0.5 bar backpressure. The conditioning protocol consisted in 5 repetitions of a potential cycle composed of 2 min at open circuit voltage (OCP), followed by 3 min at cell voltage of 0.85 V and 10 min at 0.65 V (**Figure S7**). **Figure 5** shows a summary of the lattice expansion measured *operando* after different steps of conditioning in liquid and PEMFC cells for both Faceted PtNi/C and Sponges PtNi/C catalysts compared to their pristine powders measured *ex situ*. The lattice constant expansions measured in PEMFC at 353 K were corrected from the effect of thermal expansion (*ca.* 0.006 % compared to 298 K) ⁴⁹.

Strikingly, in the case of the Faceted PtNi/C catalyst (**Figure 5.a**), a lattice expansion above 0.3 % compared to the pristine catalyst powder is observed in MEA at the very beginning of test, even before the conditioning procedure is performed. This value of lattice expansion exceeds the ones reached after any of the conditioning protocol investigated in liquid cell. This suggests the MEA manufacturing process (ink formulation, sonication, hot pressing *etc.*) causes more degradation (equivalent to 3 Ni at.% loss) than the potential cycling performed in liquid electrolyte. In fact, traces of a pure Ni phase are visible on the WAXS patterns of the pristine powder of this catalyst and still visible during all the measurements performed in liquid environment, while pure Ni is not detected anymore in the cathode catalyst layer of the MEA (see **Figure S1**). After PEMFC conditioning, the Faceted PtNi/C catalyst features a lattice expansion of 0.45 %, which translates into a loss of 4 Ni at.% from the PtNi alloy, which is more than twice what was observed after Step 1+2 in liquid cell. This suggests that, for this class of Ni-rich catalyst, the electrochemical protocol of Step 1+2 still does not fully prepare the catalyst to the corrosive environments of MEA preparation and practical PEMFC device operation. For the Sponges PtNi/C catalyst (**Figure 5.b**), MEA manufacturing also induces lattice strain relaxation of 0.16 %. However, if this value exceeds the one observed after uncomplete conditioning reached after Step 1 in the liquid cell, this is still below the value reached after Step 1+2. In fact, for this class of Ni-poor catalyst, complete conditioning in liquid cell and conditioning in PEMFC both lead to a remarkably close lattice expansion of 0.31 % (*i.e.* 2.8 % Ni at.% loss) with less than 0.6 % of error.

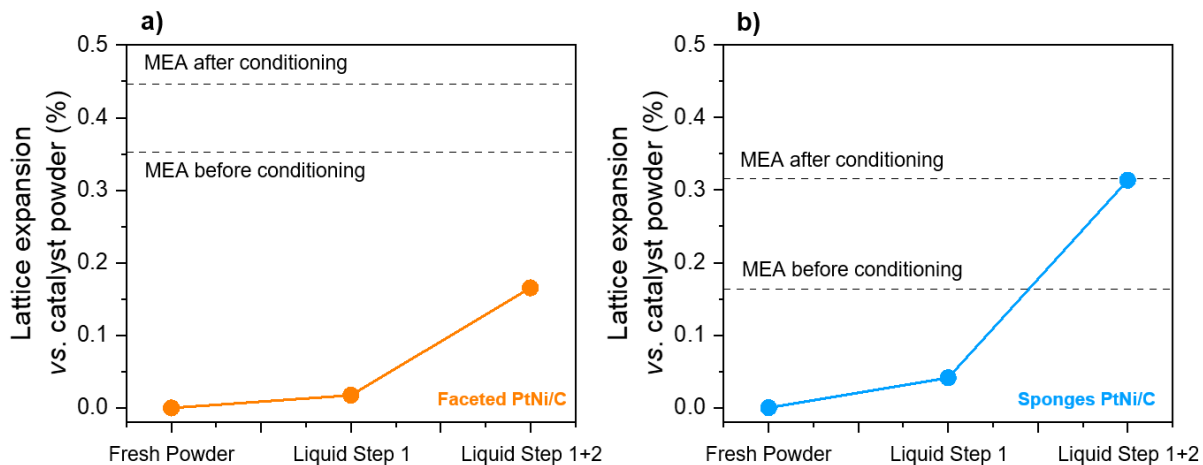


Figure 5: Lattice expansion measured operando after different steps of conditioning in liquid and PEMFC cells compared to the raw catalyst powders for a) Faceted PtNi/C and b) Sponges PtNi/C. The lattice constant expansions measured in PEMFC operando were corrected from the effect of thermal expansion (ca. 0.006 % at 353 K compared to 298 K).

All these results point toward the idea that, beyond the differences in nature of the electrolyte and structure of the catalyst layer, the viability of the conclusions obtained from model RDE experiments to practical PEMFC device regarding PtM catalyst activity for the ORR may be in great part accounted to the conditioning step. Protection of the most fragile catalysts by the application of ‘gentle’ electrochemical protocols may lead to tremendous ORR activity in RDE, which is still a highly valuable approach in fundamental science. But because PtM nanocatalyst stability in the harsh environment of PEMFC cathode is a well-established concern of primary importance, such practices in RDE are unproductive, and discredit this technique as a powerful screening method. For RDE results to possibly guide the application device development, we emphasize RDE conditioning protocol must ensure that the investigations are conducted on a realistic catalyst surface state, even if apparently unrealistic potential cycling up to 1.23 V vs. RHE may be required to achieve it. Note the apparent unrealistic upper potential limit can be seen as an approach to compensate for the unrealistic room temperature of the RDE compared to > 60 °C PEMFC, and the

crucial significance of the temperature on the non-noble metal dissolution rate^{50,51}. Thus, we propose the following steps to be implemented before any activity and/or stability measurements in RDE:

- The pre-treatment of the catalyst in 1 M aqueous H₂SO₄. The temperature and nature of the electrolyte can be adapted to the chemical nature of the PEM and the operating temperature of the device^{12,52}.
- An electrochemical conditioning protocol composed of 50 potential cycles at 500 mV s⁻¹ between 0.05 V vs. RHE and 1.23 V vs. RHE in O₂-free electrolyte.

Complementary to the recent contribution from Gatalo et al.¹² on the importance of the chemical activation of commercial PtCu/C and PtNi/C catalysts on fuel cell performance, our results suggest that catalyst candidates possibly disactivating during this conditioning protocol in RDE would likely deactivate in PEMFC at the first start-up of the device. Moreover, and in relation with the PEMFC device application, *ex situ* ‘pre-conditioning’ of the catalyst (such as the proposed systematic acidic treatment after the synthesis) has been pointed by recent works as a promising approach in limiting the contamination of the PEM by transition metal leaching during the subsequent *in situ* conditioning^{46,47,53}. While finding an appropriate way to efficiently pre-condition a PtM-rich catalyst for improved M metal retention during PEMFC operation is still an ongoing challenge, we argue that the appropriate choice of electrocatalytic materials could be an attractive alternative. As shown here with the surface-distorted Sponges PtNi/C catalyst, emerging strategies in electrocatalysts design allowing reaching reasonably high ORR activity without the use of metastable particle shape nor chemical composition^{24,25,29} should receive more attention.

CONCLUSIONS

In summary, using a combination of *operando* X-ray diffraction, online ICP-MS and RDE techniques, we have investigated in which extend Pt/C and PtNi/C fuel cell catalysts structures have to evolve in order to reach at least a temporary initial equilibrium (to be referred as beginning of life state) in the conditions of

both simulated (RDE) and practical PEMFC cathode. In agreement with former studies on Pt/C materials, our results showed that rather aggressive conditioning protocol is needed to achieve complete cleaning and stabilization of Pt surface. However, this becomes problematic for PtNi surfaces, where surface stabilization is highly entangled with early stage degradation. Our results also show significant degradations occur for PtNi catalyst between their pristine powder and (conditioned) MEA forms. This means that, to guide the development of commercial PEMFC catalysts, RDE conditioning protocol has to be adapted to be relevant for the application. The combination of acidic pre-treatment with sufficiently harsh potential cycling protocol in RDE is shown to provide a satisfactory mimicking of the catalyst initial state to be found in PEMFC. However, for the two PtNi/C catalyst investigated, this translates into an ORR activity loss of either 25 % or 66 % compared to their peak value, depending on their initial structures and chemistry. From such considerations, the study of non-noble metal-poor catalysts in which the activity does not rely on alloying effects (but rather surface distortion structural effect for example) should receive more attention. Finally, to the intuitive objection: ‘PtM catalysts may rarely see potentials as high as 1.23 V vs. RHE in the PEMFC’ one could argue ‘the surface state of PtM catalyst conditioned below 1.0 V vs. RHE in RDE may hardly see the PEMFC’.

AUTHOR INFORMATION

Corresponding Author

Raphaël Chattot, ICGM, Univ. Montpellier, CNRS, ENSCM, 34095 Montpellier Cedex 5, France.

<https://orcid.org/0000-0001-6169-530X> ; email : raphael.chattot@umontpellier.fr

ASSOCIATED CONTENT

This information is available free of charge on the ACS Publications website

Supporting Information: Details and methods about the electrocatalysts used, their synthesis, the electrochemical measurements, synchrotron wide-angle X-ray scattering measurements, Rietveld refinement, ICP analysis, TEM imaging, MEA fabrication and PEMFC tests.

ACKNOWLEDGEMENTS

We would like to thank ESRF for the provision of the beamtime at ID31 beamline as well as Helena Isern and Florian Russello for the help with the beamline preparation. R.C gratefully acknowledge financial support from the French National Research Agency through the HOLYCAT project (grant number n° ANR-22-CE05-0007). C.R., K.K., V.M., L.C., A.V, F.M. and L.D. gratefully acknowledge financial support from the French National Research Agency through the BRIDGE project (grant number n°ANR-19-ENER-0008-01). SC acknowledges IUF for financial support.

REFERENCES

- (1) Mistry, H.; Varela, A. S.; Kühl, S.; Strasser, P.; Cuenya, B. R. Nanostructured Electrocatalysts with Tunable Activity and Selectivity. *Nat. Rev. Mater.* **2016**, *1* (4), 16009.

- <https://doi.org/10.1038/natrevmats.2016.9>.
- (2) Schmidt, T. J.; Paulus, U. A.; Gasteiger, H. A.; Behm, R. J. The Oxygen Reduction Reaction on a Pt/Carbon Fuel Cell Catalyst in the Presence of Chloride Anions. *J. Electroanal. Chem.* **2001**, *508* (1–2), 41–47. [https://doi.org/10.1016/S0022-0728\(01\)00499-5](https://doi.org/10.1016/S0022-0728(01)00499-5).
 - (3) Takahashi, I.; Kocha, S. S. Examination of the Activity and Durability of PEMFC Catalysts in Liquid Electrolytes. *J. Power Sources* **2010**, *195* (19), 6312–6322. <https://doi.org/10.1016/j.jpowsour.2010.04.052>.
 - (4) Shinozaki, K.; Zack, J. W.; Richards, R. M.; Pivovar, B. S.; Kocha, S. S. Oxygen Reduction Reaction Measurements on Platinum Electrocatalysts Utilizing Rotating Disk Electrode Technique: II. Influence of Ink Formulation, Catalyst Layer Uniformity and Thickness. *J. Electrochem. Soc.* **2015**, *162* (12), F1384–F1396. <https://doi.org/10.1149/2.1071509jes>.
 - (5) Garsany, Y.; Baturina, O. A.; Swider-Lyons, K. E.; Kocha, S. S. Experimental Methods for Quantifying the Activity of Platinum Electrocatalysts for the Oxygen Reduction Reaction. In *Analytical Chemistry*; 2010; Vol. 82, pp 6321–6328. <https://doi.org/10.1021/ac100306c>.
 - (6) Shinozaki, K.; Zack, J. W.; Richards, R. M.; Pivovar, B. S.; Kocha, S. S. Oxygen Reduction Reaction Measurements on Platinum Electrocatalysts Utilizing Rotating Disk Electrode Technique. *J. Electrochem. Soc.* **2015**, *162* (10), F1144–F1158. <https://doi.org/10.1149/2.1071509jes>.
 - (7) Kocha, S. S.; Shinozaki, K.; Zack, J. W.; Myers, D. J.; Kariuki, N. N.; Nowicki, T.; Stamenkovic, V.; Kang, Y.; Li, D.; Papageorgopoulos, D. Best Practices and Testing Protocols for Benchmarking ORR Activities of Fuel Cell Electrocatalysts Using Rotating Disk Electrode. *Electrocatalysis* **2017**, *8* (4), 366–374. <https://doi.org/10.1007/s12678-017-0378-6>.

- (8) Garsany, Y.; Singer, I. L.; Swider-Lyons, K. E. Impact of Film Drying Procedures on RDE Characterization of Pt/VC Electrocatalysts. *J. Electroanal. Chem.* **2011**, *662* (2), 396–406. <https://doi.org/10.1016/j.jelechem.2011.09.016>.
- (9) Martens, S.; Asen, L.; Ercolano, G.; Dionigi, F.; Zalitis, C.; Hawkins, A.; Martinez Bonastre, A.; Seidl, L.; Knoll, A. C.; Sharman, J.; Strasser, P.; Jones, D.; Schneider, O. A Comparison of Rotating Disc Electrode, Floating Electrode Technique and Membrane Electrode Assembly Measurements for Catalyst Testing. *J. Power Sources* **2018**, *392* (January), 274–284. <https://doi.org/10.1016/j.jpowsour.2018.04.084>.
- (10) Kabir, S.; Myers, D. J.; Kariuki, N.; Park, J.; Wang, G.; Baker, A.; Macauley, N.; Mukundan, R.; More, K. L.; Neyerlin, K. C. Elucidating the Dynamic Nature of Fuel Cell Electrodes as a Function of Conditioning: An Ex Situ Material Characterization and in Situ Electrochemical Diagnostic Study. *ACS Appl. Mater. Interfaces* **2019**, *11* (48), 45016–45030. <https://doi.org/10.1021/acsami.9b11365>.
- (11) Kim, M. S.; Song, J. H.; Kim, D. K. Development of Optimal Conditioning Method to Improve Economic Efficiency of Polymer Electrolyte Membrane (PEM) Fuel Cells. *Energies* **2020**, *13* (11), 2831. <https://doi.org/10.3390/en13112831>.
- (12) Gatalo, M.; Bonastre, A. M.; Moriau, L. J.; Burdett, H.; Ruiz-Zepeda, F.; Hughes, E.; Hodgkinson, A.; Šala, M.; Pavko, L.; Bele, M.; Hodnik, N.; Sharman, J.; Gaberšček, M. Importance of Chemical Activation and the Effect of Low Operation Voltage on the Performance of Pt-Alloy Fuel Cell Electrocatalysts. *ACS Appl. Energy Mater.* **2022**, *5* (7), 8862–8877. <https://doi.org/10.1021/acsaem.2c01359>.
- (13) Yuan, X. Z.; Zhang, S.; Sun, J. C.; Wang, H. A Review of Accelerated Conditioning for a Polymer Electrolyte Membrane Fuel Cell. *J. Power Sources* **2011**, *196* (22), 9097–9106.

- <https://doi.org/10.1016/j.jpowsour.2011.06.098>.
- (14) Christmann, K.; Friedrich, K. A.; Zamel, N. Activation Mechanisms in the Catalyst Coated Membrane of PEM Fuel Cells. *Prog. Energy Combust. Sci.* **2021**, *85*, 100924. <https://doi.org/10.1016/j.pecs.2021.100924>.
- (15) Kocha, S. S.; Pollet, B. G. Advances in Rapid and Effective Break-in/Conditioning/Recovery of Automotive PEMFC Stacks. *Curr. Opin. Electrochem.* **2022**, *31*, 100843. <https://doi.org/10.1016/j.coelec.2021.100843>.
- (16) Stephens, I. E. L.; Rossmeisl, J.; Chorkendorff, I.; Ifan, B.; Lester, E.; Rossmeisl, J.; Chorkendorff, I. Toward Sustainable Fuel Cells. *Science* **2016**, *354* (6318), 1378–1380. <https://doi.org/10.1126/science.aal3303>.
- (17) Ly, A.; Asset, T.; Atanassov, P. Integrating Nanostructured Pt-Based Electrocatalysts in Proton Exchange Membrane Fuel Cells. *J. Power Sources* **2020**, *478* (August), 228516. <https://doi.org/10.1016/j.jpowsour.2020.228516>.
- (18) Ehelebe, K.; Schmitt, N.; Sievers, G.; Jensen, A. W.; Hrnjić, A.; Collantes Jiménez, P.; Kaiser, P.; Geuß, M.; Ku, Y.-P.; Jovanović, P.; Mayrhofer, K. J. J.; Etzold, B.; Hodnik, N.; Escudero-Escribano, M.; Arenz, M.; Cherevko, S. Benchmarking Fuel Cell Electrocatalysts Using Gas Diffusion Electrodes: Inter-Lab Comparison and Best Practices. *ACS Energy Lett.* **2022**, *7* (2), 816–826. <https://doi.org/10.1021/acsenerylett.1c02659>.
- (19) Alinejad, S.; Inaba, M.; Schröder, J.; Du, J.; Quinson, J.; Zana, A.; Arenz, M. Testing Fuel Cell Catalysts under More Realistic Reaction Conditions: Accelerated Stress Tests in a Gas Diffusion Electrode Setup. *JPhys Energy* **2020**, *2* (2). <https://doi.org/10.1088/2515-7655/ab67e2>.
- (20) Inaba, M.; Jensen, A. W.; Sievers, G. W.; Escudero-Escribano, M.; Zana, A.; Arenz, M.

- Benchmarking High Surface Area Electrocatalysts in a Gas Diffusion Electrode: Measurement of Oxygen Reduction Activities under Realistic Conditions. *Energy Environ. Sci.* **2018**, *11* (4), 988–994. <https://doi.org/10.1039/c8ee00019k>.
- (21) Ehelebe, K.; Seeberger, D.; Paul, M. T. Y.; Thiele, S.; Mayrhofer, K. J. J.; Cherevko, S. Evaluating Electrocatalysts at Relevant Currents in a Half-Cell: The Impact of Pt Loading on Oxygen Reduction Reaction. *J. Electrochem. Soc.* **2019**, *166* (16), F1259–F1268. <https://doi.org/10.1149/2.0911915jes>.
- (22) Ehelebe, K.; Knöppel, J.; Bierling, M.; Mayerhöfer, B.; Böhm, T.; Kulyk, N.; Thiele, S.; Mayrhofer, K. J. J.; Cherevko, S. Platinum Dissolution in Realistic Fuel Cell Catalyst Layers. *Angew. Chemie* **2021**, *133* (16), 8964–8970. <https://doi.org/10.1002/ange.202014711>.
- (23) Pinaud, B. A.; Bonakdarpour, A.; Daniel, L.; Sharman, J.; Wilkinson, D. P. Key Considerations for High Current Fuel Cell Catalyst Testing in an Electrochemical Half-Cell. *J. Electrochem. Soc.* **2017**, *164* (4), F321–F327. <https://doi.org/10.1149/2.0891704jes>.
- (24) Chattot, R.; Asset, T.; Bordet, P.; Drnec, J.; Dubau, L.; Maillard, F. Beyond Strain and Ligand Effects: Microstrain-Induced Enhancement of the Oxygen Reduction Reaction Kinetics on Various PtNi/C Nanostructures. *ACS Catal.* **2017**, *7*, 398–408. <https://doi.org/10.1021/acscatal.6b02356>.
- (25) Chattot, R.; Le Bacq, O.; Beermann, V.; Kühl, S.; Herranz, J.; Henning, S.; Kühn, L.; Asset, T.; Guétaz, L.; Renou, G.; Drnec, J.; Bordet, P.; Pasturel, A.; Eychmüller, A.; Schmidt, T. J.; Strasser, P.; Dubau, L.; Maillard, F. Surface Distortion as a Unifying Concept and Descriptor in Oxygen Reduction Reaction Electrocatalysis. *Nat. Mater.* **2018**, *17* (9), 827–833.

- (26) Chattot, R.; Martens, I.; Scohy, M.; Herranz, J.; Drnec, J.; Maillard, F.; Dubau, L. Disclosing Pt-Bimetallic Alloy Nanoparticle Surface Lattice Distortion with Electrochemical Probes. *ACS Energy Lett.* **2020**, *5* (1), 162–169. <https://doi.org/10.1021/acsenergylett.9b02287>.
- (27) Chattot, R.; Bordet, P.; Martens, I.; Drnec, J.; Dubau, L.; Maillard, F. Building Practical Descriptors for Defect Engineering of Electrocatalytic Materials. *ACS Catal.* **2020**, No. Figure 1. <https://doi.org/10.1021/acscatal.0c02144>.
- (28) Stamenkovic, V.; Mun, B. S.; Mayrhofer, K. J. J.; Ross, P. N.; Markovic, N. M.; Rossmeisl, J.; Greeley, J.; Nørskov, J. K. Changing the Activity of Electrocatalysts for Oxygen Reduction by Tuning the Surface Electronic Structure. *Angew. Chemie* **2006**, *118* (18), 2963–2967. <https://doi.org/10.1002/ange.200504386>.
- (29) Dubau, L.; Nelayah, J.; Moldovan, S.; Ersen, O.; Bordet, P.; Drnec, J.; Asset, T.; Chattot, R.; Maillard, F. Defects Do Catalysis: CO Monolayer Oxidation and Oxygen Reduction Reaction on Hollow PtNi/C Nanoparticles. *ACS Catal.* **2016**, *6* (7), 4673–4684. <https://doi.org/10.1021/acscatal.6b01106>.
- (30) Stamenkovic, V. R.; Fowler, B.; Mun, B. S.; Wang, G.; Ross, P. N.; Lucas, C. A.; Markovic, N. M. Improved Oxygen Reduction Activity on Pt₃Ni(111) via Increased Surface Site Availability. *Science* **2007**, *315* (5811), 493–497. <https://doi.org/10.1126/science.1135941>.
- (31) Calle-Vallejo, F.; Tymoczko, J.; Colic, V.; Vu, Q. H.; Pohl, M. D.; Morgenstern, K.; Loffreda, D.; Sautet, P.; Schuhmann, W.; Bandarenka, A. S. Finding Optimal Surface Sites on Heterogeneous Catalysts by Counting Nearest Neighbors. *Science* **2015**, *350* (6257), 185–189. <https://doi.org/10.1126/science.aab3501>.
- (32) Drnec, J.; Ruge, M.; Reikowski, F.; Rahn, B.; Carlà, F.; Felici, R.; Stettner, J.; Magnussen,

- O. M.; Harrington, D. A. Pt Oxide and Oxygen Reduction at Pt(111) Studied by Surface X-Ray Diffraction. *Electrochem. commun.* **2017**, *84* (September), 50–52. <https://doi.org/10.1016/j.elecom.2017.10.002>.
- (33) Abbou, S.; Chattot, R.; Martin, V.; Claudel, F.; Solà-Hernandez, L.; Beauger, C.; Dubau, L.; Maillard, F. Manipulating the Corrosion Resistance of SnO₂ Aerogels through Doping for Efficient and Durable Oxygen Evolution Reaction Electrocatalysis in Acidic Media. *ACS Catal.* **2020**, *10* (13), 7283–7294. <https://doi.org/10.1021/acscatal.0c01084>.
- (34) Ruge, M.; Drnec, J.; Rahn, B.; Reikowski, F.; Harrington, D. A.; Carlà, F.; Felici, R.; Stettner, J.; Magnussen, O. M. Structural Reorganization of Pt(111) Electrodes by Electrochemical Oxidation and Reduction. *J. Am. Chem. Soc.* **2017**, *139* (12), 4532–4539. <https://doi.org/10.1021/jacs.7b01039>.
- (35) Jacobse, L.; Huang, Y. F.; Koper, M. T. M.; Rost, M. J. Correlation of Surface Site Formation to Nanoisland Growth in the Electrochemical Roughening of Pt(111). *Nat. Mater.* **2018**, *17* (3), 277–282. <https://doi.org/10.1038/s41563-017-0015-z>.
- (36) Bard, A. J.; Faulkner, L. R. Effect of Adsorption of Electroinactive Species. In *Electrochemical Methods: Fundamentals and Applications*; John Wiley & Sons, Inc., 2001; pp 569–571.
- (37) Chattot, R.; Martens, I.; Mirolo, M.; Ronovsky, M.; Russello, F.; Isern, H.; Braesch, G.; Hornberger, E.; Strasser, P.; Sibert, E.; Chatenet, M.; Honkimäki, V.; Drnec, J. Electrochemical Strain Dynamics in Noble Metal Nanocatalysts. *J. Am. Chem. Soc.* **2021**, *143* (41), 17068–17078. <https://doi.org/10.1021/jacs.1c06780>.
- (38) Martens, I.; Chattot, R.; Rasola, M.; Blanco, M. V.; Honkimäki, V.; Bizzotto, D.; Wilkinson, D. P.; Drnec, J. Probing the Dynamics of Platinum Surface Oxides in Fuel Cell

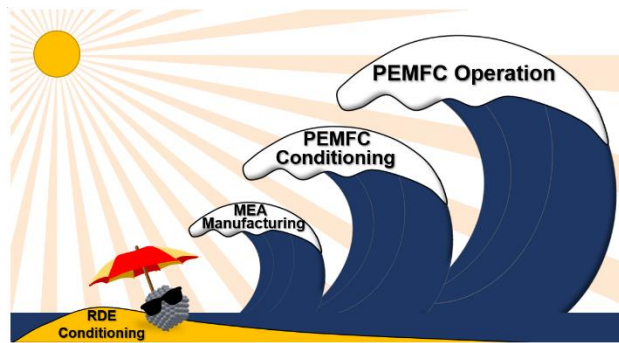
- Catalyst Layers Using in Situ X-Ray Diffraction. *ACS Appl. Energy Mater.* **2019**, *2* (11), 7772–7780. <https://doi.org/10.1021/acsaem.9b00982>.
- (39) Markovic, N. M.; Ross, P. N. Surface Science Studies of Model Fuel Cell Electrocatalysts. *Surf. Sci. Rep.* **2002**, *45* (4–6), 117–229. [https://doi.org/10.1016/s0167-5729\(01\)00022-x](https://doi.org/10.1016/s0167-5729(01)00022-x).
- (40) Marichev, V. A. Reversibility of Platinum Voltammograms in Aqueous Electrolytes and Ionic Product of Water. *Electrochim. Acta* **2008**, *53* (27), 7952–7960. <https://doi.org/10.1016/j.electacta.2008.05.076>.
- (41) Van Der Niet, M. J. T. C.; Garcia-Araez, N.; Hernández, J.; Feliu, J. M.; Koper, M. T. M. Water Dissociation on Well-Defined Platinum Surfaces: The Electrochemical Perspective. *Catal. Today* **2013**, *202*, 105–113. <https://doi.org/10.1016/j.cattod.2012.04.059>.
- (42) Janik, M. J.; McCrum, I. T.; Koper, M. T. M. On the Presence of Surface Bound Hydroxyl Species on Polycrystalline Pt Electrodes in the “Hydrogen Potential Region” (0–0.4 V-RHE). *Journal of Catalysis*. Academic Press Inc. November 1, 2018, pp 332–337. <https://doi.org/10.1016/j.jcat.2018.09.031>.
- (43) Garcia-Araez, N.; Climent, V.; Feliu, J. M. Analysis of Temperature Effects on Hydrogen and OH Adsorption on Pt(1 1 1), Pt(1 0 0) and Pt(1 1 0) by Means of Gibbs Thermodynamics. *J. Electroanal. Chem.* **2010**, *649* (1–2), 69–82. <https://doi.org/10.1016/j.jelechem.2010.01.024>.
- (44) Topalov, A. A.; Cherevko, S.; Zeradjanin, A. R.; Meier, J. C.; Katsounaros, I.; Mayrhofer, K. J. J. Towards a Comprehensive Understanding of Platinum Dissolution in Acidic Media. *Chem. Sci.* **2014**, *5* (2), 631–638. <https://doi.org/10.1039/c3sc52411f>.
- (45) You, H.; Zurawski, D. J.; Nagy, Z.; Yonco, R. M. In-Situ x-Ray Reflectivity Study of Incipient Oxidation of Pt(111) Surface in Electrolyte Solutions. *J. Chem. Phys.* **1994**, *100*

- (6), 4699–4702. <https://doi.org/10.1063/1.466254>.
- (46) Gatalo, M.; Jovanovič, P.; Petek, U.; Šala, M.; Šelih, V. S.; Ruiz-Zepeda, F.; Bele, M.; Hodnik, N.; Gaberšček, M. Comparison of Pt-Cu/C with Benchmark Pt-Co/C: Metal Dissolution and Their Surface Interactions. *ACS Appl. Energy Mater.* **2019**, *2* (5), 3131–3141. <https://doi.org/10.1021/acsaem.8b02142>.
- (47) Moriau, L. J.; Hrnjić, A.; Pavlišič, A.; Kamšek, A. R.; Petek, U.; Ruiz-Zepeda, F.; Šala, M.; Pavko, L.; Šelih, V. S.; Bele, M.; Jovanovič, P.; Gatalo, M.; Hodnik, N. Resolving the Nanoparticles' Structure-Property Relationships at the Atomic Level: A Study of Pt-Based Electrocatalysts. *iScience* **2021**, *24* (2). <https://doi.org/10.1016/j.isci.2021.102102>.
- (48) Martens, I.; Vamvakeros, A.; Chattot, R.; Blanco, M. V.; Rasola, M.; Pusa, J.; Jacques, S. D. M.; Bizzotto, D.; Wilkinson, D. P.; Ruffmann, B.; Heidemann, S.; Honkimäki, V.; Drnec, J. X-Ray Transparent Proton-Exchange Membrane Fuel Cell Design for in Situ Wide and Small Angle Scattering Tomography. *J. Power Sources* **2019**, *437*, 226906. <https://doi.org/10.1016/j.jpowsour.2019.226906>.
- (49) Arblaster, J. W. Crystallographic Properties of Platinum. *Platin. Met. Rev.* **1997**, *41* (1), 12–21. <https://doi.org/10.1595/147106713X665030>.
- (50) Đukić, T.; Moriau, L. J.; Pavko, L.; Kostelec, M.; Prokop, M.; Ruiz-Zepeda, F.; Šala, M.; Dražić, G.; Gatalo, M.; Hodnik, N. Understanding the Crucial Significance of the Temperature and Potential Window on the Stability of Carbon Supported Pt-Alloy Nanoparticles as Oxygen Reduction Reaction Electrocatalysts. *ACS Catal.* **2022**, *12* (1), 101–115. <https://doi.org/10.1021/acscatal.1c04205>.
- (51) Dubau, L.; Maillard, F. Unveiling the Crucial Role of Temperature on the Stability of Oxygen Reduction Reaction Electrocatalysts. *Electrochem. commun.* **2016**, *63*, 65–69.

<https://doi.org/10.1016/j.elecom.2015.12.011>.

- (52) Han, B.; Carlton, C. E.; Kongkanand, A.; Kukreja, R. S.; Theobald, B. R.; Gan, L.; O'Malley, R.; Strasser, P.; Wagner, F. T.; Shao-Horn, Y. Record Activity and Stability of Dealloyed Bimetallic Catalysts for Proton Exchange Membrane Fuel Cells. *Energy Environ. Sci.* **2015**, *8* (1), 258–266. <https://doi.org/10.1039/C4EE02144D>.
- (53) Gatalo, M.; Moriau, L.; Petek, U.; Ruiz-Zepeda, F.; Šala, M.; Grom, M.; Galun, T.; Jovanovič, P.; Pavlišič, A.; Bele, M.; Hodnik, N.; Gaberšček, M. CO-Assisted Ex-Situ Chemical Activation of Pt-Cu/C Oxygen Reduction Reaction Electrocatalyst. *Electrochim. Acta* **2019**, *306*, 377–386. <https://doi.org/10.1016/j.electacta.2019.03.153>.

TABLE OF CONTENTS/ABSTRACT GRAPHICS



For Table of Contents Only